Large-eddy simulation of rotating channel flows using a localized dynamic model

Ugo Piomelli and Junhui Liu
Department of Mechanical Engineering, University of Maryland, College Park, Maryland 20742

Most applications of the dynamic subgrid-scale stress model use volume- or planar-averaging to avoid ill-conditioning of the model coefficient, which may result in numerical instabilities. Furthermore, a spatially-varying coefficient is mathematically inconsistent with the original derivation of the model. A localization procedure is proposed here that removes the mathematical inconsistency to any desired order of accuracy in time. This model is applied to the simulation of rotating channel flow, and results in improved prediction of the turbulence statistics. The model coefficient vanishes in regions of quiescent flow, reproducing accurately the intermittent character of the flow on the stable side of the channel. Large-scale longitudinal vortices can be identified, consistent with the observation from experiments and direct simulations. The effect of the unresolved scales on higher-order statistics is also discussed. © *1995 American Institute of Physics.*

I. INTRODUCTION

The dynamic subgrid-scale stress model, introduced by Germano *et al.*[1] has been widely used for the large-eddy simulation (LES) of incompressible and compressible flows. The model is based on the introduction of two filters; in addition to the *grid* filter (denoted by an overbar), which defines the resolved and subgrid scales, a *test* filter (denoted by a circumflex) is used, whose width is larger than the grid filter width. The stress terms that appear when the grid filter is applied to the Navier-Stokes equations are the subgrid-scale (SGS) stresses τ_{ij}; in an analogous manner, the test filter defines a new set of stresses, the subtest-scale stresses T_{ij}. An identity[2] relates T_{ij} and τ_{ij} to the resolved turbulent stresses, $\mathscr{L}_{ij}$. If an eddy-viscosity model is used to parametrize τ_{ij} and T_{ij}, this identity can be exploited[1,3] to determine the model coefficient.

This yields a coefficient that is function of space and time, and whose value is determined by the energy content of the smallest resolved scales, rather than input *a priori* as in the standard Smagorinsky model.[4] Two difficulties, however, arise in the determination of C: the first is that the model is ill-conditioned because the denominator of the expression for C becomes very small at a few points in the flow. Furthermore, the procedure described above is not mathematically self-consistent since it requires that a spatially-dependent coefficient be extracted from a filtering operation.[5] To overcome this problem, C is usually assumed to be only a function of time and of the spatial coordinates in inhomogeneous directions. The mathematical inconsistency is thus eliminated, and the ill-conditioning problem is alleviated.

The resulting eddy viscosity has several desirable features: it vanishes in laminar flow, it can be negative (indicating that the model is capable of predicting backscatter, i.e., energy transfer from the small to the large scales) and it has the correct asymptotic behavior near a solid boundary. The dynamic eddy viscosity model has been used successfully to solve a variety of flows such as transitional and turbulent channel flows,[1,5,6] and compressible flows.[7–9] Since the model coefficient adjusts itself to the energy content of the smallest resolved scales, this model can also be applied to relaminarizing or intermittent flows, and has given accurate prediction of problems in which the Smagorinsky model did not work well. Esmaili and Piomelli,[10] who used it for the LES of sink flows, observed that C vanishes when the boundary layer relaminarizes even if inactive fluctuations are still present. Squires and Piomelli[11] applied it to rotating flows, and found that C decreases as a result of the stabilizing effect of rotation.

Orszag *et al.*[12] moved a number of criticisms to the dynamic model. In the first place, they attributed its success in the prediction of low Reynolds number flows to the fact that it acts as a damping function for the eddy viscosity in the wall region; they state that, near the wall, the test filter width $\hat{\Delta}$ is in the inertial range and the grid filter width $\bar{\Delta}$ is in the dissipation range, resulting in $T_{ij} \ll \tau_{ij}$ and $\langle\mathscr{L}_{ij}\rangle \simeq \langle\tau_{ij}\rangle \sim y^3$ ($\langle \cdot \rangle$ denotes plane-averaging). It is easy to show analytically that this conjecture is incorrect since, for most filters of interest, $\langle T_{ij}\rangle \geqslant \langle\tau_{ij}\rangle$ independent of the shape of the spectrum. Furthermore, in the wall region, both $\bar{\Delta}$ and $\hat{\Delta}$ are in flat regions of the spectrum, and the ratios of $\mathscr{L}_{ij}$, T_{ij}, and τ_{ij} to the resolved energy and stresses become constant, as shown in Ref. 6. Orszag and coworkers[12] also state that the model depends very strongly on the ratio of test to grid filter width, a point that had already been addressed by Germano *et al.*,[1] who showed that the LES results are rather insensitive to this ratio, a result confirmed by Spyropoulos and Blaisdell.[12] Finally, Orszag *et al.*[12] conjecture that application of the model may become problematic at high Reynolds numbers; however, Piomelli[6] and Balaras *et al.*[13] have computed channel flow at Reynolds numbers (based on channel width and bulk velocity) ranging between 5000 and 250 000 (200<Re<5000 based on channel halfwidth and friction velocity), obtaining results in good agreement with the data.

A limitation of the dynamic model is, however, the plane averaging mentioned above. For flows in which no homogeneous directions exist, the model coefficient should be a

function of all spatial coordinates. Even flows that are homogeneous in planes parallel to the wall may be intermittent, in which case the eddy viscosity should be non-zero only in regions of significant turbulent activity, and zero elsewhere, a behavior that is not always possible if plane averaging is performed. Thus, to allow the application of the dynamic model to flows of engineering interest it is essential to develop a localized formulation of the model.

Although straightforward localization of the dynamic model gives rise to the problems mentioned above, it has nonetheless been used by Zang and coworkers in simulations of the turbulent flow in a driven cavity.[14] They performed local averaging over the test filter cell, and constrained the total viscosity (sum of molecular and eddy viscosity) to be non-negative, thus allowing a small amount of backscatter. Since large (positive and negative) values of the eddy viscosity were observed only in the corner of the cavity, probably due to the low Reynolds number of the flow they studied, neither the local averaging nor the cutoff applied to avoid backscatter affected the results very much. In later work[15] the same authors adopted a mixed model that was also localized in a similar manner.

Ghosal and coworkers[16] recast the problem in variational form, obtaining an integral equation for C that they solved iteratively. Their formulation, to which they refer as the "Dynamic Localization Model" (DLM), removed the mathematical inconsistency, as well as the ill-conditioning that led to locally large values of C; negative values of the model coefficient were avoided by the additional constraint that $C \geqslant 0$. This model was used for the LES of isotropic decay[16] and to study the flow over a backward-facing step,[16,17] with results in good agreement with DNS data. Carati *et al.*[18] also applied the DLM to homogeneous isotropic turbulence, with a separate backscatter model. Although the DLM has given promising results in a variety of flows, the overhead associated with the iterative solution of the integral equation can be significant.

The purpose of this paper is to demonstrate the accuracy of a new localized version of the dynamic model in which the mathematical inconsistency is removed only approximately (i.e., to some order of accuracy in time). The present formulation, however, does not require any iteration; thus, its cost, in terms of CPU and memory, is essentially the same as the plane-averaged model. A small amount of backscatter can be allowed, but negative total viscosities are avoided for numerical stability.

To evaluate the new localized model, it will be used for the computation of rotating channel flow. Rotating channel flow is an attractive test for subgrid-scale models because system rotation has some important effects on turbulence: for instance, it inhibits energy transfer from large to small scales; this leads to a reduction in turbulence dissipation and a decrease in the decay rate of turbulence energy. Furthermore, the turbulence length scales along the rotation axis increase relative to those in non-rotating turbulence. The presence of mean shear normal to the axis of rotation may have either a stabilizing or a destabilizing effect, depending on whether the angular velocity and mean shear have the same or opposite signs. In turbulent channel flow, for ex-

ample, system rotation acts to both stabilize and destabilize the flow. On the unstable side Coriolis forces resulting from system rotation enhance turbulence-producing events, leading to an increase in turbulence levels, while on the stable side Coriolis forces inhibit turbulence production and decrease turbulence levels. The increase in the component energies, however, is dependent on the rotation rate: at sufficiently high rotation rates streamwise fluctuations on the unstable channel wall are suppressed relative to the non-rotating case. The stabilizing/destabilizing effects of rotation on turbulence in channel flow make this problem particularly challenging, since the SGS model is required to capture relaminarization with inactive turbulent motions as well as fully-developed turbulence.

Because of the interesting physical phenomena that occur when a turbulent plane channel flow is subjected to system rotation, this flow has been investigated experimentally,[19] and numerically (by direct[20] and large-eddy[21] simulations). The focus of this article, therefore, will not be the description of the flow physics, which have already been studied quite extensively in the cited references, but rather the response of the localized model to the physical phenomena that characterize this flow, a response to which the better prediction capabilities of this model can be attributed.

In the next section, the numerical method will be discussed; then the model will be presented and applied to the simulation of rotating channel flow. The results will then be discussed, and conclusions and recommendations for future work will be drawn.

II. NUMERICAL METHOD

In large-eddy simulations the flow variables are decomposed into a large scale (or resolved) component, denoted by an overbar, and a subgrid scale component. The large scale component is defined by the filtering operation:

$$\bar{f}(\mathbf{x}) = \int_D f(\mathbf{x}') \bar{G}(\mathbf{x}, \mathbf{x}') d\mathbf{x}', \tag{1}$$

where D is the computational domain, and $\bar{G}$ is the filter function.

Appling the filtering operation to the incompressible Navier-Stokes and continuity equations yields the filtered equations of motion,

$$\frac{\partial \bar{u}_i}{\partial t} + \frac{\partial}{\partial x_j}(\bar{u}_i \bar{u}_j) = -\frac{1}{\rho}\frac{\partial \bar{p}}{\partial x_i} - \frac{\partial \tau_{ij}}{\partial x_j} + \nu \frac{\partial^2 \bar{u}_i}{\partial x_j \partial x_j}$$
$$+ 2\epsilon_{ij3}\Omega \bar{u}_j, \tag{2}$$

$$\frac{\partial \bar{u}_i}{\partial x_i} = 0, \tag{3}$$

where ϵ_{ijk} is Levi-Civita's alternating tensor and Ω the angular velocity of the system. The axis of rotation is in the positive z, or x_3 direction. The subgrid-scale stresses, $\tau_{ij} = \overline{u_i u_j} - \bar{u}_i \bar{u}_j$, need to be modeled to represent the effect of the subgrid scales on the resolved field. Since the small

U. Piomelli and J. Liu

scales tend to be more isotropic than the large scales, their effects can be modeled by fairly simple eddy viscosity models of the form[3]

$$\tau_{ij} - \frac{\delta_{ij}}{3}\tau_{kk} = -2\nu_T \bar{S}_{ij} = -2C\bar{\Delta}^2|\bar{S}|\bar{S}_{ij}, \tag{4}$$

in which δ_{ij} is Kronecker's delta, $\bar{\Delta}$ is the length scale, related to the filter width (see below) and $|\bar{S}| = (2\bar{S}_{ij}\bar{S}_{ij})^{1/2}$ is the magnitude of the large-scale strain rate tensor

$$\bar{S}_{ij} = \frac{1}{2}\left(\frac{\partial\bar{u}_i}{\partial x_j} + \frac{\partial\bar{u}_j}{\partial x_i}\right). \tag{5}$$

The trace of the subgrid-scale stresses is incorporated in the pressure term. The method used to compute the coefficient C will be described in the next section. The filter widths $\bar{\Delta}$ and $\hat{\Delta}$ are given by

$$\bar{\Delta} = (\bar{\Delta}_1\bar{\Delta}_2\bar{\Delta}_3)^{1/3}; \quad \hat{\Delta} = (\hat{\Delta}_1\hat{\Delta}_2\hat{\Delta}_3)^{1/3}, \tag{6}$$

where $\bar{\Delta}_i$ is the grid spacing in the ith direction, and $\hat{\Delta}_1 = 2\bar{\Delta}_1$, $\hat{\Delta}_2 = \bar{\Delta}_2$, $\hat{\Delta}_3 = 2\bar{\Delta}_3$. Since the filter width in the wall-normal direction is the same as the grid filter width, the test filter is in practice applied only in the homogeneous directions.

The governing equations (2) and (3) are integrated in time using a Fourier-Chebyshev pseudospectral collocation scheme.[22] The skew-symmetric form of the momentum equation (2) is employed, and the time-advancement is performed by a fractional time step method with a semi-implicit scheme; the wall-normal diffusion term is advanced using the Crank-Nicolson scheme, and the remaining terms by a low-storage third-order Runge-Kutta scheme. Periodic boundary conditions are applied in the streamwise (x) and spanwise (z) directions, and no-slip conditions at the solid walls. No dealiasing is performed. The computational domain in the streamwise, wall-normal and spanwise directions is $4\pi\delta \times 2\delta \times 4\pi\delta/3$ (where δ is the channel halfwidth).

III. APPROXIMATE LOCALIZATION

The dynamic model is based on an identity relating the resolved turbulent stresses $\mathscr{L}_{ij} = \widehat{\bar{u}_i\bar{u}_j} - \widehat{\bar{u}}_i\widehat{\bar{u}}_j$ to the subgrid- and subtest-scale stresses[2]:

$$\mathscr{L}_{ij} = T_{ij} - \widehat{\tau_{ij}}, \tag{7}$$

where $T_{ij} = \widehat{\overline{u_i u_j}} - \widehat{\bar{u}}_i\widehat{\bar{u}}_j$. The subgrid- and subtest-scale stresses are then parameterized by eddy viscosity models of the form (4):

$$\tau_{ij} - \frac{\delta_{ij}}{3}\tau_{kk} = -2C\bar{\Delta}^2|\bar{S}|\bar{S}_{ij} = -2C\beta_{ij}, \tag{8}$$

$$T_{ij} - \frac{\delta_{ij}}{3}T_{kk} = -2C\hat{\Delta}^2|\hat{\bar{S}}|\hat{\bar{S}}_{ij} = -2C\alpha_{ij}. \tag{9}$$

Substituting (8) and (9) into (7) yields

$$\mathscr{L}^a_{ij} = \mathscr{L}_{ij} - \frac{\delta_{ij}}{3}\mathscr{L}_{kk} = -2C\alpha_{ij} + 2\widehat{C\beta_{ij}}. \tag{10}$$

This is a set of five independent equations that cannot be solved explicitly for C, which appears inside a filtering op-

eration. If, however, one assumes that $C = C(y,t)$, then $\widehat{C\beta_{ij}} = C\widehat{\beta_{ij}}$. The sum of the squares of the residual,

$$E_{ij} = \mathscr{L}^a_{ij} + 2C\alpha_{ij} - 2C\widehat{\beta_{ij}}, \tag{11}$$

can then be minimized by contracting both sides of (10) with $\alpha_{ij} - \widehat{\beta}_{ij}$ to yield:[22]

$$C(y,t) = -\frac{1}{2}\frac{\langle\mathscr{L}^a_{ij}(\alpha_{ij} - \widehat{\beta}_{ij})\rangle}{\langle(\alpha_{mn} - \widehat{\beta}_{mn})(\alpha_{mn} - \widehat{\beta}_{mn})\rangle}, \tag{12}$$

where $\langle\cdot\rangle$ denotes plane-averaging. This form of the coefficient has been widely used in LES calculations. In studies of homogeneous isotropic turbulence, averaging is performed over the entire computational domain, and $C = C(t)$ only, whereas averaging over the spanwise direction is used for spatially-developing flows.

As mentioned above, a straightforward localization of the model was used in Refs. 14 and 15, in which C was given by (12) with the plane-averaging replaced by a local average over the test filter cell. The problem of the mathematical inconsistency of the localized application of (12) is not addressed in that work, but the results are in good agreement with experimental data; however, the Reynolds number of those calculations is quite low, and the SGS contribution to the stresses is rather small, which makes it difficult to draw definite conclusions from those simulations.

Ghosal and coworkers[16] noted that, if C is assumed to be fully dependent on space, the residual cannot be minimized in the least-squares sense locally; therefore, they introduced a constrained variational problem consisting of the minimization of the integral of the square of the sum of the residuals over the entire domain, with the additional constraint that C be non-negative. The result was of the form of Fredholm's integral equation of the second kind; they solved the integral problem iteratively using under-relaxation to improve convergence. The solution of the integral equation is similar to the solution of the Poisson equation for the pressure, and can be rather expensive: Carati et al.[18] estimated that the calculation of the DLM model coefficient requires four times the CPU time necessary for the plane-averaged dynamic model coefficient. Since the calculation of the eddy viscosity with the present code requires approximately 15% of the total CPU time, the iterative scheme could increase the cost of a calculation by over 50%.

In the present work a simpler approach is followed: the expression (10) is recast in the form

$$-2C\alpha_{ij} = \mathscr{L}^a_{ij} - 2\widehat{C^*\beta_{ij}}, \tag{13}$$

where on the right-hand side an estimate of the coefficient, denoted by C^* and assumed to be known, is used. Since C^* is known, the sum of the squares of the residual can now be minimized locally; the contraction that minimizes it, in this case, is:

$$C = -\frac{1}{2}\frac{(\mathscr{L}^a_{ij} - 2\widehat{C^*\beta_{ij}})\alpha_{ij}}{\alpha_{mn}\alpha_{mn}}. \tag{14}$$

The denominator of (14) is positive definite, like that of (12), but has the advantage that it does not involve a difference between two terms of the same order of magnitude. In wall-

Phys. Fluids, Vol. 7, No. 4, April 1995

U. Piomelli and J. Liu   841

TABLE I. Summary of the numerical calculations.

Case	Re_τ	Re_b	Ro_τ	Ro_b	Model	Grid	$u_{\tau b}/u_{\tau 0}$	$u_{\tau t}/u_{\tau 0}$
0	177	5 700	1.14	0.144	DNS	$96\times97\times128$	1.17	0.80
1	181	5 700	1.14	0.144	Plane-averaged	$32\times65\times48$	1.15	0.82
2	175	5 700	1.18	0.144	Zeroth-order	$32\times65\times48$	1.18	0.77
3	192	5 700	0.00	0.000	First-order	$32\times65\times48$	1.00	1.00
4	185	5 700	0.54	0.069	First-order	$32\times65\times48$	1.13	0.85
5	176	5 700	1.17	0.144	First-order	$32\times65\times48$	1.17	0.79
6	185	5 700	1.63	0.210	First-order	$32\times65\times48$	1.20	0.75
7	320	11 500	1.93	0.210	First-order	$48\times65\times64$	1.19	0.76
8	540	23 000	2.25	0.210	First-order	$48\times65\times64$	1.17	0.79

bounded flows, $\alpha_{mn}\alpha_{mn}$ becomes small only where the mean shear vanishes (in the free stream of a boundary layer, for example); the numerator is also expected to vanish there. In these regions, moreover, the flow is essentially uniform, so that spurious high values of C obtained from the ratio of very small numbers should not result in large values of the eddy viscosity or of the SGS stresses. This conjecture was verified *a posteriori* (see below).

There are various ways to obtain C^* at time-step n:

(1) Use the value at the previous time-step:

$$C^* = C^{n-1}. \tag{15}$$

(2) Estimate the value at the present time-step by some backward extrapolation scheme:

$$C^* = C^{n-1} + \Delta t \left.\frac{\partial C}{\partial t}\right|_{n-1} + \cdots . \tag{16}$$

(3) Use an iterative scheme: set $C^* = C^{n-1}$ and calculate the left-hand side of (14); then replace C^* with the newly obtained value and repeat the procedure until convergence to the desired order of accuracy is reached.

Since the cost of an iterative scheme would be similar to that of the DLM model of Ghosal *et al.*,[16] the first and second approaches, whose cost is the same as the plane-averaged model, will be taken in this work; a first-order extrapolation scheme will be used in which $\partial C/\partial t|_{n-1}$ is evaluated using an explicit Euler scheme:

$$\left.\frac{\partial C}{\partial t}\right|_{n-1} = \frac{C^{n-1} - C^{n-2}}{t_{n-1} - t_{n-2}}, \tag{17}$$

which gives

$$C^* = C^{n-1} + \frac{t_n - t_{n-1}}{t_{n-1} - t_{n-2}}(C^{n-1} - C^{n-2}). \tag{18}$$

Equation (15) will be referred to as the "zeroth-order approximation," Eq. (18) as the "first-order approximation". No attempt was made to use higher-order schemes, since little difference was observed between the results obtained with the first- and zeroth-order approximations.

Use of an extrapolation scheme such as the one proposed here contains some inherent dangers: numerical instabilities are possible, and the difference between C^* and the actual value C^n could be quite large if C varied on a short time-scale. In practice, however, C is a fairly slowly-varying func-

tion of time because of the temporal filtering introduced implicitly by the spatial filtering. By eliminating the smallest scales of motion, the highest frequencies are also filtered out. Typically, the time-scale of the structures whose length scale is the filter width is 5 to 10 times larger than the time-step, and this results in long correlation times for C.[23]

The coefficient C obtained from (15) or (18) can be either positive or negative. Since negative total viscosities that are correlated over long times can lead to numerical instabilities, the total viscosity was constrained to be nonnegative. For the extrapolation (15) and (18) the constrained value was used. Numerical tests showed no significant difference if the unconstrained value was employed in the extrapolation. Finally, since the coefficient C appears in the modeling of the subtest stresses T_{ij}, it should be smooth over a scale $\hat{\Delta}$. To ensure this, it was locally averaged over the test cell.

IV. RESULTS AND DISCUSSION

Calculations were performed for a range of Reynolds numbers $Re_b = U_b(2\delta)/\nu$ (based on the channel width, 2δ, and bulk velocity, U_b), and rotation numbers $Ro_b = \Omega(2\delta)/U_b$. A summary of the calculations is shown in Table I [the last two columns in Table I show the ratio of the friction velocity u_τ on the stable (subscript t) and unstable (subscript b) sides to the friction velocity in absence of rotation, $u_{\tau 0}$]. The grid resolution for the various cases was chosen on the basis of the results of Ref. 5, to ensure that the SGS stresses gave a significant contribution to the momentum transport, while the grid filter cutoff remained in the decaying region of the spectra, except very near the wall. The initial conditions for the cases with non-zero rotation rates were obtained from equilibrium cases at $\Omega = 0$, and were in very good agreement with experimental and DNS data.[6] After rotation was applied the simulations were integrated forward in time to a new steady state, and the statistics were obtained by averaging over at least 4 dimensionless time units tu_τ/δ. The sample size was considered satisfactory when the total shear stress deviated by less than 0.5% from the expected linear behavior.

Experimental measurements in this flow exist[19] at higher Reynolds numbers. A series of DNS calculations was performed by Kristoffersen and Andersson[20] that span the range of Ro_b examined in this work. A direct simulation of the intermediate ($Ro_b = 0.144$) case was also performed to com-
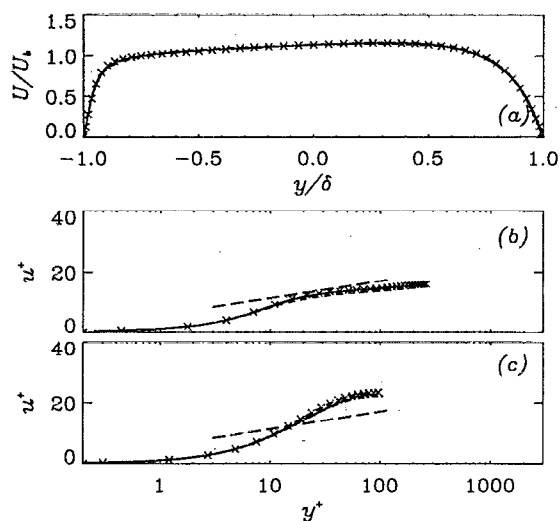
FIG. 1. Mean velocity in the rotating channel. $Re_b = 5700$, $Ro_b = 0.144$. —— First-order; - - - zeroth order; —·— plane-averaged; — — 2.5 log $y^+ + 5.0$; × DNS (only every other point is shown). (a) Global coordinates; (b) wall coordinates, unstable side; (c) wall coordinates, stable side.

pare with the LES results. The DNS used $96 \times 97 \times 128$ grid points, and was in very good agreement with the DNS results of Ref. 20; a DNS on a finer mesh ($128 \times 129 \times 128$) was also performed, but the statistical sample accumulated was insufficient; the results obtained with the two DNS calculations were in very good agreement.

The mean velocity profiles for cases 1, 2, and 5 (i.e., the calculations for $Re_b = 5700$ and $Ro_b = 0.144$) are compared with DNS data in Fig. 1. Very little difference can be observed between the various results. The localized models, however, give better prediction of the turbulent fluctuations $u_i'' = \bar{u}_i - \langle \bar{u}_i \rangle$ (where $\langle \cdot \rangle$ from here on denotes averaging over planes parallel to the wall and time), than the plane-averaged model, especially on the stable side of the channel (Fig. 2).

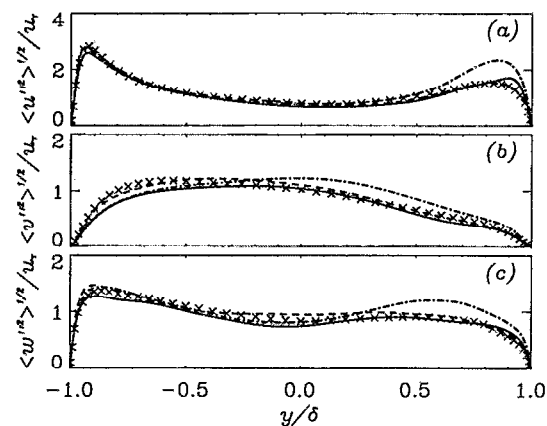The average values of C are shown in Fig. 3. There is very little difference between the zeroth- and first-order ap-

FIG. 2. Turbulence intensities in the rotating channel. $Re_b = 5700$, $Ro_b = 0.144$. —— First-order; - - - zeroth order; —·— plane-averaged; × DNS (only every other point is shown). (a) u; (b) v; (c) w.
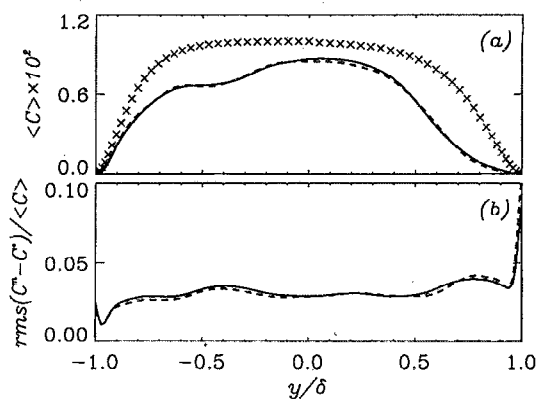

FIG. 3. Average model coefficient. $Re_b = 5700$, $Ro_b = 0.144$. —— First-order; - - - zeroth order; × Smagorinsky coefficient $C_s^2[1 - \exp(-y^+/25)]^2$. (a) $\langle C \rangle$; (b) RMS difference.

proximations. The localized models are slightly more dissipative than the plane-averaged one (in which backscatter acts to lower the plane-averaged C). The root-mean-square (RMS) difference between the predicted coefficient C^* and the actual value C^n is also shown in Fig. 3(b) (normalized by the average C). The difference is fairly small (less than 5%) throughout the channel, except on the stable side, where it increases because of the low value of $\langle C \rangle$; almost no difference can be observed between the zeroth- and first-order approximations, perhaps because of the high temporal correlation of the coefficient. The square of the Smagorinsky constant multiplied by the Van Driest damping function, $C_s^2[1 - \exp(-y^+/25)]^2$, is also shown for reference. Although the local u_τ, i.e., the value on the nearest wall, is used in the evaluation of y^+, the Smagorinsky constant is significantly higher than the dynamic model coefficient, especially on the stable side of the channel. Furthermore, the asymptotic behavior of the length scale as $y^+ \to 0$ is incorrect (see also Ref. 5).

The average value of C is lower on the unstable than on the stable side, as expected; the maximum value of C corresponds to a Smagorinsky constant $C_s \approx 0.09$. As the rotation number is increased (Fig. 4), the region on the stable side where C is small becomes wider, reflecting the more quiescent character of the flow there. The SGS stress on the unstable side (Fig. 5) is slightly larger than in the zero rotation rate (about 10% of the resolved ones vs 8% in the no-rotation case) while on the stable side it reaches about half the value
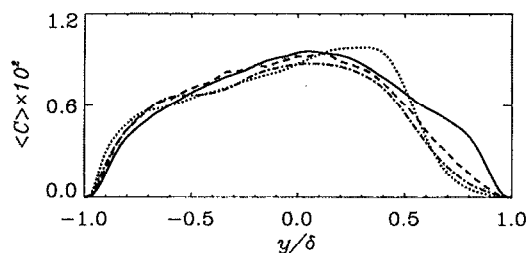

FIG. 4. Average model coefficient. $Re_b = 5700$. —— $Ro_b = 0$; - - - $Ro_b = 0.069$; —·— $Ro_b = 0.144$; ······ $Ro_b = 0.21$.

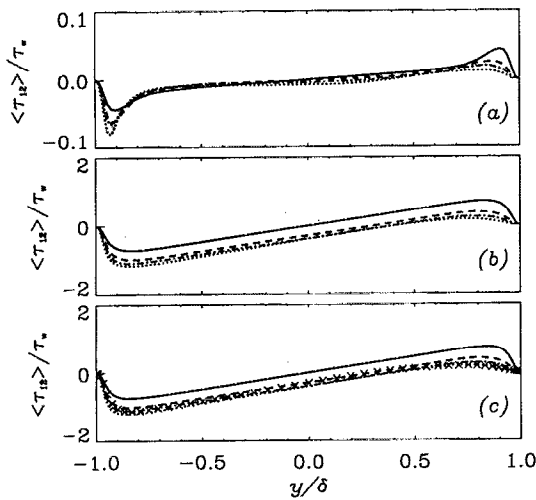Phys. Fluids, Vol. 7, No. 4, April 1995

U. Piomelli and J. Liu   843

FIG. 5. Subgrid-scale and resolved shear stresses, $Re_b = 5700$. ——
$Ro_b = 0$; – – – $Ro_b = 0.069$; –·– $Ro_b = 0.144$; ······ $Ro_b = 0.21$; × DNS,
$Ro_b = 0.144$ (only every other point is shown). (a) Subgrid scale; (b) re-
solved; (c) resolved+subgrid-scale.

it has when no rotation is applied. As the rotation number is
increased, the SGS stress increases on the unstable side and
decreases on the stable side, but it never vanishes entirely as
it would if the flow relaminarized completely.

Full relaminarization on the stable side was observed in
experiments[19] and in the LES calculations of Tafti and
Vanka;[21] in the DNS calculations of Kristoffersen and
Andersson[20] and in the present ones, however, the fluctua-
tions on the stable side remained significant, and the mean
velocity never reached the laminar profile, even at large ro-
tation rates and at a Reynolds number at which relaminariza-
tion is expected to occur. The friction velocity u_τ normalized
by the friction velocity in the absence of rotation $u_{\tau 0}$, is
shown in Fig. 6 (the results of the numerical calculations are
also tabulated in Table I). The LES, DNS, and experimental
data are in good agreement on the unstable side; in the ex-
periment the bulk velocity was obtained from the volume
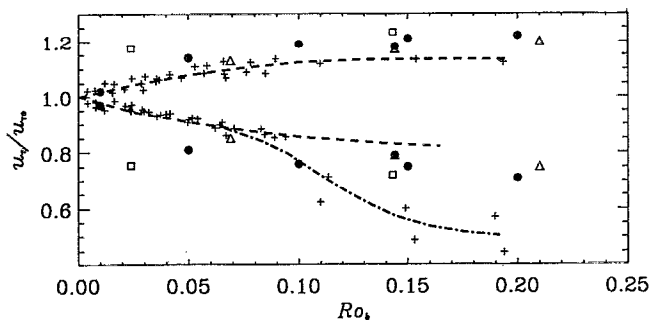flow rate, which led to an underestimation of the bulk veloc-

FIG. 6. Friction velocity on the two sides of the channel. + Experiments,
Johnston et al.;[19] ● DNS (present simulation and results by Kristofferssen
and Andersson[20]); □ LES, Smagorinsky model, Tafti and Vanka;[21] △ LES,
present calculation, $Re_b = 5700$. The lines are correlations of experimental
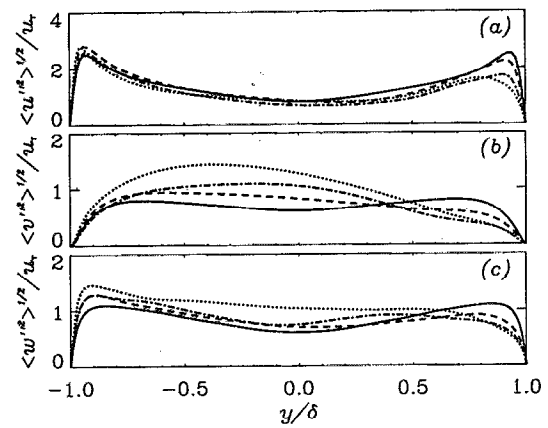data from Ref. 19.

FIG. 7. Turbulence intensities in the rotating channel, $Re_b = 5700$. ——
$Ro_b = 0.0$, – – – $Ro_b = 0.069$, –·– $Ro_b = 0.144$, ······ $Ro_b = 0.210$. (a) u; (b)
v; (c) w.

ity (and an overestimation of Ro_b) because of the presence of
boundary layers on the sides of the channel (see also Ref.
20).

A more significant difference can be observed on the
stable side, where the numerical results tend to lie close to
the extrapolation of the results of experiments in which the
flow remained turbulent on the stable side (the dashed line),
and are significantly higher than those for fully relaminarized
flow (the chain-dot line). Possible reasons for the difference
between the experimental and DNS results on the stable side
are the relatively small aspect ratio of the experimental ap-
paratus and the fact that the flow was not fully developed,
which may have added a streamwise pressure gradient that
could have increased the tendency of the flow towards
relaminarization. The results obtained with the dynamic
model are in much better agreement with the DNS than those
obtained by Tafti and Vanka[21] with the Smagorinsky model;
in that calculation the increased dissipation of the SGS
model due to the higher values of the constant shown above,
coupled perhaps with the numerical dissipation due to the
finite-differencing scheme, resulted in excessive damping of
the fluctuations on the stable side and excessively low wall
stress even at the lower rotation rate they examined.

The turbulence intensities normalized by the average
friction velocity for various rotation rates are shown in Fig.
7. The DNS results of Ref. 20 show that, on the unstable
side, the peak RMS streamwise fluctuation is maximum for
$Ro_b \simeq 0.1$ and then decreases; the present calculations show
the same trend.

At the high rotation rates the formation of roll cells
could be observed from $v-w$ velocity vectors in the cross-
plane. The roll cells had also been observed in experiments
and numerical simulations. Usually, two strong cells are
present, accompanied, sometimes, by two weaker ones. The
vortical structures tend to drift both in the y and z directions
(see also Ref. 20). The vortices convect high momentum
fluid in the downwash region between them, and, as they
drift towards the stable wall, the wall stress there can fluctu-
ate significantly. While on the unstable wall the friction ve-
locity (Fig. 8) is nearly constant in time, on the stable wall it
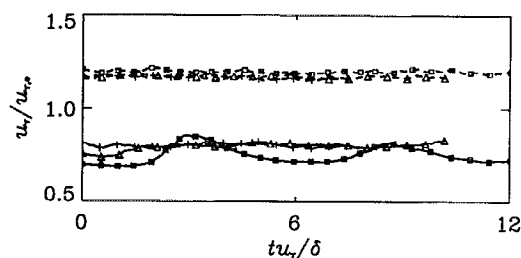exhibits an oscillation with a period of about 4 tu_τ/δ time

U. Piomelli and J. Liu

FIG. 8. History of the friction velocity on the upper and lower walls, $Ro_b = 0.210$. □ Re_b = 5700; △ Re_b = 11 500; + Re_b = 23 000. —— Stable wall, – – – unstable wall.

FIG. 10. Model coefficient contours in the xz-plane. $Re_b = 5700$, $Ro_b = 0.210$, $tu_\tau / \delta = 8.98$, $y^+ = 5.4$. (a) Unstable wall; (b) stable wall. Contour lines are at intervals of $\pm 5 \times 10^{-4}$; dashed lines indicate positive contours.

units, and with significant amplitude. It should be remarked here that use of LES allows to integrate the governing equations for very long times compared with DNS: in the calculations shown in Fig. 8, for instance, statistics were obtained typically by averaging over a period of 9 δ/u_τ units ($3 < tu_\tau / \delta < 12$) compared with only $3.2 u_\tau / \delta$ in the DNS in Ref. 20.

Figure 9 shows contours of the u'' velocity fluctuations in two xz-planes near the unstable and stable walls at $tu_\tau / \delta = 8.98$ (near a local maximum of u_τ). On the unstable side the elongated streaky structure typical of wall-bounded flows is present. On the stable side, the downwash of the roll cells appears as an elongated region of increased u'' velocity fluctuations at $z^+ \simeq 500$, as also observed in the direct simulations (see, for instance, Fig. 17 in Ref. 20). The v'' fluctuations and the Reynolds stresss $u'' v''$ (not shown) exhibit similar behavior. To illustrate the response of the localized model to this motion, contours of the model coefficient C are shown in Fig. 10. The coefficient varies very significantly over the plane; on the stable side, larger values of C are observed where the velocity fluctuations are also large (i.e., in the downwash region of the roll cells); regions of backscatter (indicated by solid lines) can be observed.

When the roll cells move away from the stable wall the velocity fluctuations in the near-wall layer become extremely small (Fig. 11), and the near-wall layer on the stable side
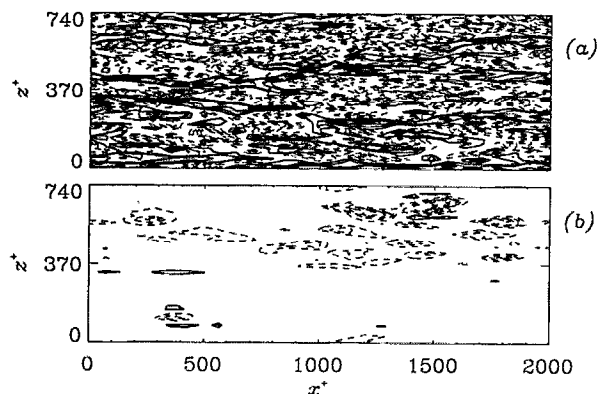
becomes quasi-laminar. The model coefficient (Fig. 12) also becomes very small: the contour levels in Fig. 12(b) are one order of magnitude smaller than in the other figures.

As mentioned above, the present localization is better-behaved than the straightforward localization of Eq. (12). With the present technique the coefficient rarely exceeds 20 times its mean value, except near the stable wall, where $|C| > 20 \langle C \rangle$ at 3% of the grid points due to the fact that the flow there is very quiescent, with small regions of localized turbulent activity. For comparison, if (12) were localized by replacing the plane average with averaging over the test filter width, $|C| > 20 \langle C \rangle$ at 30% of the grid points. In this case, most spurious values appear near the channel center, where the mean shear is small; this effect might be due to the type of filtering used, and might be less pronounced if, for instance, a tophat filter in real space were employed.

The velocity skewness and flatness factors obtained from the DNS and the first-order model are compared in Figs. 13 and 14. These statistics were computed after the calculation was completed, using only the velocity fields that had been

FIG. 9. Streamwise velocity fluctuation contours in the xz-plane. $Re_b = 5700$, $Ro_b = 0.210$, $tu_\tau / \delta = 8.98$, $y^+ = 5.4$. (a) Unstable wall; (b) stable wall. Contour lines are at intervals of ± 1; dashed lines indicate positive contours.
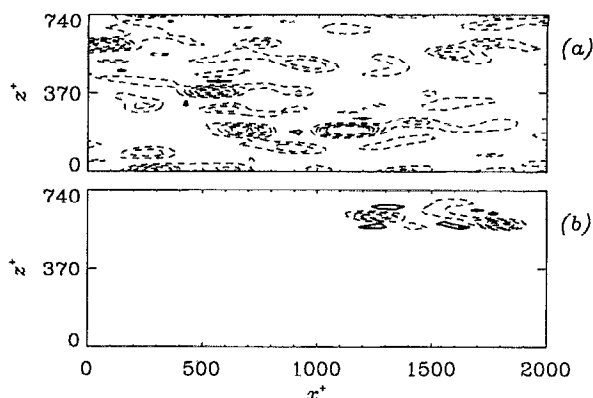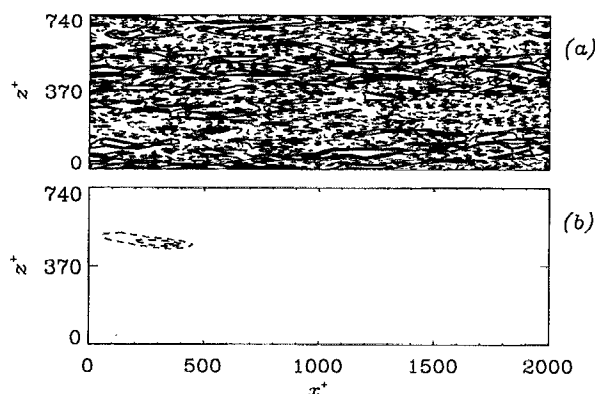

FIG. 11. Streamwise velocity fluctuation contours in the xz-plane. $Re_b = 5700$, $Ro_b = 0.210$, $tu_\tau / \delta = 6.16$, $y^+ = 5.4$. (a) Unstable wall; (b) stable wall. Contour lines are at intervals of ± 1; dashed lines indicate positive contours.

Phys. Fluids, Vol. 7, No. 4, April 1995
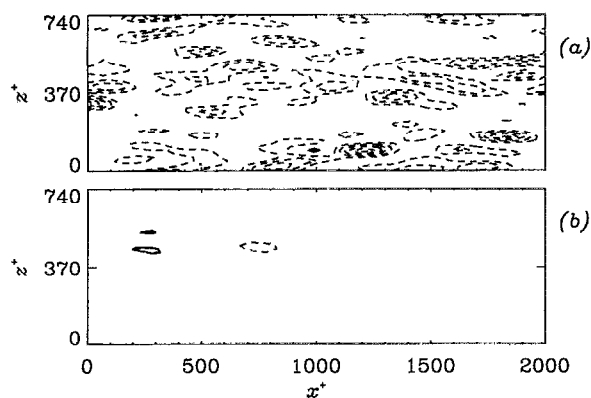
U. Piomelli and J. Liu   845

FIG. 12. Model coefficient contours in the xz-plane. $Re_b = 5700$, $Ro_b = 0.210$, $tu_\tau/\delta = 6.16$, $y^+ = 5.4$. (a) Unstable wall; (b) stable wall. Contour lines are at intervals of $\pm 5 \times 10^{-4}$ in part (a), $\pm 5 \times 10^{-5}$ in part (b); dashed lines indicate positive contours.

stored every $tu_\tau/\delta = 0.1$, whereas the other statistics shown were obtained by sampling the data at intervals $tu_\tau/\delta = 0.025$; the sample size is, therefore, not completely satisfactory, as shown by the small non-zero skewness of the spanwise velocity component w for the DNS. On the unstable side, the present LES follow the same trends discussed in Ref. 6: the LES predicts slightly higher skewness than the DNS, but the overall agreement between LES and DNS data is quite good. On the stable side the flatness and skewness are significantly increased as an effect of rotation, due to the highly intermittent character of the flow on the stable side. The wall-normal component has the highest flatness, because of the large values of v fluctuations associated with the fluid that is convected towards the wall by the roll cells. Similar phenomena were also observed by Tafti and Vanka.[21]

The LES on the stable side predicts the correct trends, but the flatness and skewness of all the velocity components are much lower than the DNS values. To find the reason for
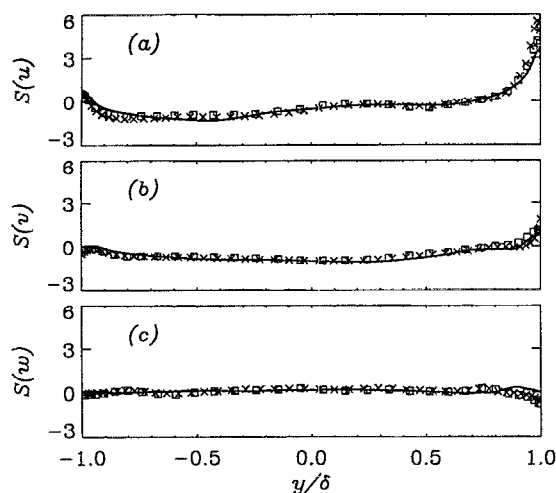

FIG. 13. Velocity skewness in the rotating channel. $Re_b = 5700$, $Ro_b = 0.144$. —— First-order; $\times$ DNS (only every other point is shown); $\square$ filtered DNS. (a) u; (b) v; (c) w.
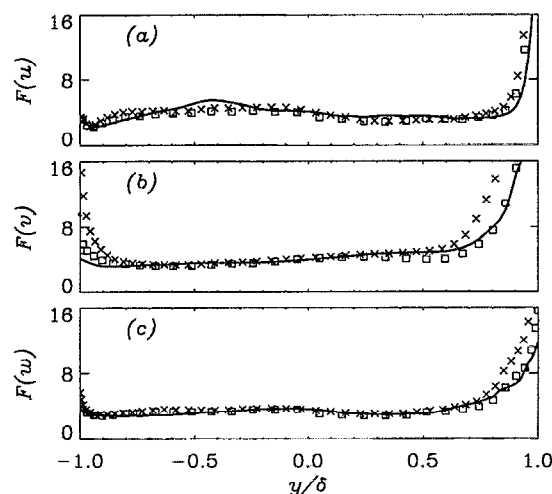

FIG. 14. Velocity flatness in the rotating channel. $Re_b = 5700$, $Ro_b = 0.144$. —— First-order; $\times$ DNS (only every other point is shown); $\square$ filtered DNS. (a) u; (b) v; (c) w.

this discrepancy, the DNS data was filtered on a grid with $32 \times 65 \times 48$ points, the same as that used in the LES. The agreement between LES data and filtered DNS data is very good on both sides of the channel, confirming the conjecture by Piomelli[6] that the contribution of the unresolved turbulent scales accounts for the difference between DNS and LES data.

Two calculations were performed at higher Reynolds numbers, $Re_b = 11\,300$ and $23\,000$. The mesh was refined only slightly in these calculations (see Table I); in outer coordinates it was finer than for the low Reynolds number case; in wall units, however, the spanwise grid size was $\Delta z^+ = 18.5$, 24, and 41 on the unstable side, respectively, for the low, intermediate, and high Reynolds numbers, cases 6, 7, and 8; such spacing is sufficient to capture most of the turbulent events that take place there. On the stable side, where the flow is more quiescent and the local Reynolds number lower, the grid resolution issue is less critical.

As the Reynolds numbers is increased, the roll cells become less well-defined (see Ref. 19), and that is reflected in a less dramatic variation of the friction velocity with time on the stable side of the channel (Fig. 8). At the highest Reynolds number very little oscillation can be observed, a result consistent with those of Johnston and coworkers,[19] who observed that roll cells were present only for Reynolds numbers in the range $6000 < Re < 15\,000$.

The mean velocity profiles in wall coordinates are not much altered by increasing the Reynolds umber (Fig. 15), except for the lengthening of the logarithmic layer with increasing Reynolds number. The ratio $u_\tau/u_{\tau 0}$ is also nearly unaffected by the Reynolds number.

The turbulence intensities at the three Reynolds numbers are shown in Fig. 16. The main difference among the various calculations is the thinning of the inner layer, evidenced by a movement of the maximum turbulence intensities towards the wall. In wall coordinates the maximum of the streamwise turbulence intensities is at $y^+ \simeq 15$ on the unstable side,
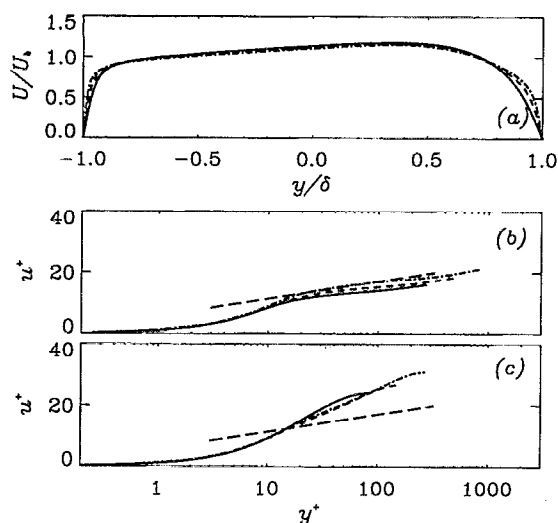
U. Piomelli and J. Liu

FIG. 15. Mean velocity in the rotating channel, $Ro_b = 0.21$. —— $Re_b = 5700$; – – – $Re_b = 11\,500$; —·— $Re_b = 23\,000$; – – – $2.5 \log y^+ + 5.0$. (a) Global coordinates; (b) wall coordinates, unstable side; (c) wall coordinates, stable side.

$y^+ \simeq 20$ on the stable side, irrespective of Reynolds number.

V. CONCLUDING REMARKS

A new localization procedure for the dynamic eddy-viscosity model has been proposed. The localization is only approximate, in the sense that it is based on a Taylor series expansion of the model coefficient in which the time derivatives are evaluated numerically. This allows to compute a localized coefficient at negligible additional cost compared with the plane-averaged formulation. Nonetheless, it results in more accurate results compared with the plane-averaged formulation of the model. The localization proposed here, moreover, is better conditioned than the original formulation, and does not result in numerical instabilities.

The proposed localization has been tested by computing the flow in a rotating channel. Although the grids used are very coarse, the localized model predicts statistics in good agreement with DNS data; some discrepancy between all the numerical results (both DNS and LES) and the experiments can be explained based on the different boundary conditions. First-order accurate localization, which can be performed with little increase in cost or memory, appears sufficient to reduce the mathematical inconsistency to acceptable levels. The fact that the model coefficient is governed by the time scale of the resolved field results in a high correlation (in time) of the coefficient; this feature allows a simple extrapolation procedure such as the one used here to give accurate results.

Mean velocity and rms turbulence intensities predicted by the LES agree well with the DNS data. The skewness and flatness of the velocity components computed from the LES were compared with those obtained from the DNS. The LES data showed the same trends as the fine DNS data; the effect of the unresolved scales was highlited by comparing the LES data with DNS data filtered on the same grid used by the LES. The agreement between the LES and the filtered DNS quantities was excellent.

The vortical structures that are characteristic of rotating flows of this type were captured. Their time evolution has significant effects on the flow field, especially on the stable side of the channel. The localized model adapts to the intermittent nature of the flow: on the stable side, it is non-zero only in the downwash region of the roll cells, where the turbulent fluctuations are also significant; when the roll cells move away from the stable wall, the coefficient nearly vanishes on the stable side.

[1] M. Germano, U. Piomelli, P. Moin, and W. H. Cabot, "A dynamic subgrid-scale eddy viscosity model," Phys. Fluids A **3**, 1760 (1991).

[2] M. Germano, "Turbulence: the filtering approach," J. Fluid Mech. **238**, 325 (1992).

[3] D. K. Lilly, "A proposed modification of the Germano subgrid-scale closure method," Phys. Fluids A **4**, 633 (1992).

[4] J. Smagorinsky, "General circulation experiments with the primitive equations. I. The basic experiment," Mon. Weather Rev. **91**, 99 (1963).

[5] W. H. Cabot, and P. Moin, "Large eddy simulation of scalar transport with the dynamic subgrid-scale model," in *Large Eddy Simulation of Complex Engineering and Geophysical Flows*, edited by B. Galperin and S. A. Orszag (Cambridge University Press, Cambridge, 1993), p. 141.

[6] U. Piomelli, "High Reynolds number calculations using the dynamic subgrid-scale stress model," Phys. Fluids A **5**, 1484 (1993).

[7] P. Moin, K. D. Squires, W. H. Cabot, and S. Lee, "A dynamic subgrid-scale model for compressible turbulence and scalar transport," Phys. Fluids A **3**, 2746 (1991).

[8] N. M. El-Hady, T. A. Zang, and U. Piomelli, "Application of the dynamic subgrid-scale model to axisymmetric transitional boundary layer at high speed," Phys. Fluids **6**, 1299 (1994).

[9] E. T. Spyropoulos, and G. A. Blaisdell, "Evaluation of the dynamic subgrid-scale model for large-eddy simulations of compressible turbulent flows," AIAA Paper No. 95-0355, 1995.

[10] H. Esmaili, and U. Piomelli, "Large-eddy simulation of relaminarizing sink flow boundary layers," in *Near-Wall Turbulent Flows*, edited by R. M. C. So, C. G. Speziale, and B. E. Launder (Elsevier, Amsterdam, 1993), p. 287.

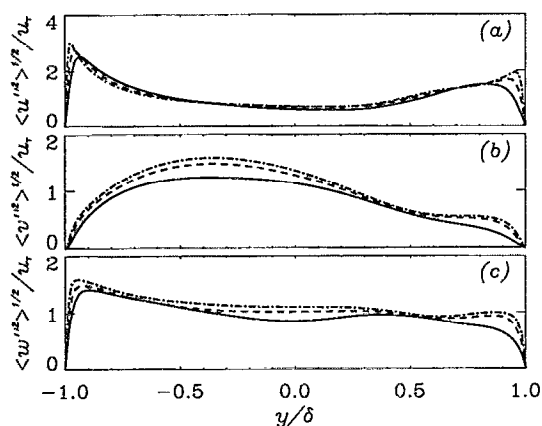[11] K. D. Squires and U. Piomelli, "Dynamic modeling of rotating turbu-

FIG. 16. Turbulence intensities in the rotating channel, $Ro_b = 0.21$. $Re_b = 5700$; – – – $Re_b = 11\,500$; $Re_b = 23\,000$. (a) u; (b) v; (c) w.

Phys. Fluids, Vol. 7, No. 4, April 1995

U. Piomelli and J. Liu   847

lence," *Turbulent Shear Flows 9*, edited by F. Durst, N. Kasagi, B. E. Launder, F. W. Schmidt, and J. H. Whitelaw (Springer-Verlag, Heidelberg, 1995), p. 73.

[12] S. A. Orszag, I. Staroselsky, and V. Y. Yakhot, "Some basic challenges for large eddy simulation research," in *Large Eddy Simulation of Complex Engineering and Geophysical Flows*, edited by B. Galperin and S. A. Orszag (Cambridge University Press, Cambridge, 1993), p. 55.

[13] E. Balaras, C. Benocci, and U. Piomelli, "Finite difference computations of high Reynolds number flows using the dynamic subgrid-scale model." Theoret. Comput. Fluid Dyn. (in press, 1995).

[14] Y. Zang, R. L. Street, and J. Koseff, "Application of a dynamic subgrid-scale model to turbulent recirculating flows," in *Annual Research Briefs – 1992* (Center for Turbulence Research, Stanford University, 1993), p. 85.

[15] Y. Zang, R. L. Street, and J. Koseff, "A dynamic mixed subgrid-scale model and its application to turbulent recirculating flows," Phys. Fluids A **5**, 3186 (1993).

[16] S. Ghosal, T. S. Lund, P. Moin, and K. Akselvoll, "A dynamic localization model for large-eddy simulation of turbulent flows," J. Fluid Mech. (in press, 1995).

[17] K. Akselvoll, and P. Moin, "Application of the dynamic localization model to large-eddy simulation of turbulent flow over a backward facing step," in *Engineering Applications of Large Eddy Simulations–1993*, edited by S. A. Ragab and U. Piomelli (The American Society of Fluids Engineering, New York, 1993), p. 1.

[18] D. Carati, S. Ghosal, and P. Moin, "On the representation of backscatter in dynamic localization models," submitted to Phys. Fluids.

[19] J. P. Johnston, R. M. Halleen, and D. K. Lezius, "Effects of spanwise rotation on the structure of two-dimensional fully developed turbulent channel flow," J. Fluid Mech. **56**, 533 (1972).

[20] R. Kristoffersen and H. I. Andersson, "Direct simulation of low Reynolds number turbulent flow in a rotating channel," J. Fluid Mech. **256**, 163 (1993).

[21] D. K. Tafti and S. P. Vanka, "A numerical study of the effects of spanwise rotation on turbulent channel flow," Phys. Fluids A **3**, 642 (1991).

[22] T. A. Zang and M. Y. Hussaini, "On spectral multigrid methods for the time-dependent Navier-Stokes equations," Appl. Math. Comp. **19**, 359 (1986).

[23] T. Lund, S. Ghosal, and P. Moin, "Numerical experiments with highly-variable eddy viscosity models," in *Engineering Applications of Large Eddy Simulations–1993*, edited by S. A. Ragab and U. Piomelli (The American Society of Fluids Engineering, New York, 1993), p. 7.